LUNAR SUBSURFACE EXPLORATION WITH COHERENT RADAR

WALTER E. BROWN, JR.
California Institute of Technology, Jet Propulsion Laboratory, Pasadena, Calif. U.S.A.

Abstract. The Apollo Lunar Sounder Experiment that is scheduled to orbit the Moon on Apollo 17 consists of a three frequency coherent radar system and an optical recorder. The coherent radar can be used to measure both phase and amplitude characteristics of the radar echo. Measurement methods that are related to the phase and amplitude will be used to determine the surface profile, locate subsurface features and ascertain near surface electrical properties of the lunar surface. The key to the coherent radar measurement is a highly stable oscillator that preserves an accurate phase reference (2 or 3 electrical degrees) over a long period of time. This reference provides a means for reducing surface clutter so that subsurface features are more easily detected and also provides a means of measuring range to the surface to within a fraction of a wavelength.

1. Introduction

An interesting combination of electromagnetic sounding and sidelooking radar measurement techniques will be used on a remote sensing sounding experiment which is scheduled for flight on the Apollo 17. The primary purpose of the Apollo Lunar Sounder Experiment (S-209) is to search for subsurface features from the orbiting Command and Service Module (CSM). From this vantage point, 110 km above the surface, and traveling at velocities in excess of 1.6 km/s the sounder experiment will scan a path about 43000 km long on the lunar surface. The sensitivity of the measurement is such that it will detect a layer-like dielectric discontinuity of 1.3 to 1 at depths as great as 1 km.

Other major objectives of the S-209 experiment include the acquisition of a continuous profile of the lunar surface, a mapping of surface electrical properties and an areal map of some subsurface scatterers. It is expected that the Lunar Sounder data will add significantly to the geological, geophysical and geographical understanding of the Moon. The experiment has been designed with this premise in mind and with a realistic understanding of the spacecraft capabilities and limitations.

The purpose of this paper is to discuss the coherent radar measurement techniques and to show how and why certain types of performance can be expected from the Lunar Sounder instrument. The major S-209 experiment parameters are pertinent to the measurement method and are given in Table I.

A coherent radar is defined, for our purposes, as a radar that attributes all unpredicted variations in echo amplitude and phase to a characteristic of the target and none to the radar system or transmission medium. Whenever the situation deviates from this assumption the radar loses some coherence. All processes from transmission to echo display are designed to be *linear*. Cross-product terms in the radar transfer functions must be suppressed by 60 to 70 dB, otherwise a strong surface response will

Communication presented at the Conference on Lunar Geophysics, held between October 18–21, 1971, at the Lunar Science Institute in Houston, Texas, U.S.A.

TABLE I

Major parameters of the Apollo lunar sounder experiment (S–209)

Weight	Radar 44 lbs.	Recorder 107 lbs.	Antenna 68 lbs.	Total 219 lbs.
Power	Radar 126 W	Recorder 110 W		Total 236 W

Frequency	Pulse width	Pulse repetition rate	Wavelength
5– 5.5 MHz	240 μs	400	60 m
15–16.6 MHz	80 μs	400	20 m
150–166	8 μs	2000	2 m

Operational Mode

Altitude	110 km
5 and 15 MHz	2 orbits
Cooling Period	2 orbits
150 MHz	2 orbits
Listen only (5 and 15 MHz)	2 orbits or more

Antenna HF 30 m tip-to-tip
VHF Yagi 20° off vertical/cross track

Data Systems

Optical Recorder–film (recovered EVA)
Some digital data is handled via the Apollo data handling system

cause a weak subsurface echo to be unrecoverable in the post-flight data processing. The principle mode of subsurface detection is in the time domain, hence, the sidelobe levels of the first surface echo must be minimized and therefore, the phase transfer function of the radar system must be linear. The amplitude and phase of each echo are recorded for subsequent ground-based processing, where any combination of filtering may be accomplished. With the amplitude and phase of the echo recorded in a linear fashion, the mission may be 'reflown' in search of 'new' subsurface features as often as the data analyst chooses.

In summary, the coherent radar is defined as a radar that has (a) a highly stable oscillator, (b) highly linear transfer functions in both amplitude and phase and (c) a method for recording the amplitude and phase of each echo.

2. Surface Measurement Aspects

To examine some of the more interesting properties of the coherent radar, particularly as they apply to a sounding system, one might consider the radar response to those targets first located on the surface and secondly to those beneath the surface. This section deals with the surface response. A target will have a Doppler frequency history and an amplitude history as the spacecraft passes the target. With both amplitude and phase recorded, the problem of focusing on the target becomes one of using matched filter techniques when the recorded data is processed. The azimuth resolution obtained

is limited by the length of the Doppler frequency history as weighted by the amplitude history. If the amplitude history is uniform the azimuth resolution would be equivalent to that obtained by an antenna as long as the distance traveled by the spacecraft during the acquisition of the Doppler history. The maximum nominal acquisition period for the Lunar Sounder is 10 s or about 16000 m. Hence, the equivalent maximum length of the antenna (synthetic aperture) is 16000 m! The equivalent beamwidth on the surface will, in this case, be about 5 wavelengths. This factor is very important in reducing azimuthal surface clutter. If the surface is smooth, then the azimuthal spot would then be equivalent to the diameter (d) of the first Fresnel zone or

$$\begin{aligned} d &= 5150 \text{ m} \quad & \lambda &= 60 \text{ m} \\ d &= 2970 \text{ m} \quad & \lambda &= 20 \text{ m} \\ d &= 940 \text{ m} \quad & \lambda &= 2 \text{ m} \end{aligned}$$

and surface clutter is no longer a problem.

In range, the dimension orthogonal to the Doppler, the maximum radar resolution is established by the bandwidth of the transmitted pulse. For each of the three Lunar Sounder frequencies, the bandwidth was taken to be a nominal 10% of the carrier frequency. The matched filter (to achieve low sidelobes) yields a resolution of 10 wavelengths (the wavelength as measured in the propagation medium). In free space, the resolution, r, is

$$\begin{aligned} r &= 600 \text{ m} \quad & \lambda &= 60 \text{ m} \\ r &= 200 \text{ m} \quad & \lambda &= 20 \text{ m} \\ r &= 20 \text{ m} \quad & \lambda &= 2 \text{ m} \end{aligned}$$

Two other aspects of range performance have a significant bearing on the overall performance of the Lunar Sounder S-209, the absolute range accuracy and the so-called range dimension of the footprint. The absolute range accuracy, as derived in the Appendix, is determined by the equation

$$\sigma_R = \frac{1}{B(\text{SNR})^{1/2}} \frac{c}{2}, \tag{2.1}$$

if the assumption is made that surface behaves unpredictably from one integration interval to the next, and where B = Bandwidth = carrier frequency ÷ 10; SNR = output signal power to noise power ratio; c = velocity of light in the propagation medium.

For the Lunar Sounder parameters and expected performance over a smooth surface

$$\begin{aligned} \sigma_R &= 2 \text{ cm} \quad & \lambda &= 2 \text{ m} \\ \sigma_R &= 12 \text{ cm} \quad & \lambda &= 20 \text{ m} \\ \sigma_R &= 21 \text{ cm} \quad & \lambda &= 60 \text{ m} \end{aligned}$$

The values for the Zone SNR_0 in Table II were used for these calculations.

The actual ranging errors will be somewhat larger because the surface is not smooth and the electron density between the spacecraft and the lunar surface will cause some additional error particularly for the 2 m wavelength. For the longer wavelengths, the

TABLE II

Signal to noise ratios in dB

1 λ(m)	2 RF SNR_1	3 Recorder SNR_2	4 $SNRI_1$ Compress	5 $SNRI_2$ Zone target	6 $SNRI_3$ Point target	7 $SNRI_0$ Zone target
60	24	15	17	31.1	36	63
20	22	11	17	28.6	36	56
2	18	6	17	30.7	43	54

This table is a summary of the S–209 performance at an altitude of 110 km above the lunar surface.
Column 1 is the operating wavelength.
Column 2 is the signal-to-noise ratio (SNR) into the optical recorder for a planar target.
Column 3 is the SNR after the signal has been recorded on film.
Column 4 is the SNR improvement resulting from pulse compression and includes the matched filter loss.
Column 5 is the SNR improvement resulting from the linear addition of pulses during the interval of time required cross a Fresnel zone.
Column 6 is the SNR improvement over a 10 second aperture for a point target.
Column 7 is the output SNR for a Fresnel zone target.

simultaneous transmission allows the lunar ionospheric error to be cancelled out. With an electron density of 10 electrons/cc the range difference between the 5 MHz and 15 MHz echoes is about 140 cm. This range difference will fluctuate with variations in electron density and disappear on the dark side of the moon.

The range dimension of the areal footprint is equivalent to the Fresnel zone diameter at vertical incidence for a smooth surface. However, for a rough surface the dimension is limited by the effective pulse width and at vertical incidence it is given by

$$y = 2(hc\alpha)^{1/2} = 2(10h\lambda)^{1/2}. \tag{2.2}$$

The second form is for the Lunar Sounder case where the bandwidth is 10 percent of the carrier frequency and where h=altitude, c=velocity of light, α=pulse width (equivalent).

The cross-track footprint dimension at vertical incidence is

$$y = 16300 \text{ m} \quad \lambda = 60 \text{ m}$$
$$y = 9400 \text{ m} \quad \lambda = 20 \text{ m}$$
$$y = 2980 \text{ m} \quad \lambda = 2 \text{ m}$$

References have been made herein to a smooth surface. For purposes of this paper, a smooth surface is defined as one which has a vertical incidence specular-to-diffuse energy ratio greater than 30 dB or the rms uncertainty in phase in the diffraction pattern generated by a particular surface element is less than 1/60th of a wavelength.

A typical Doppler and amplitude history of the echoes from a surface element is illustrated in Figure 1. The envelope is actually an array of samples taken at the pulse repetition frequency (PRF). It is important that the PRF exceed the highest significant Doppler frequency by at least a factor of two to avoid ambiguities. Although the peak

of the amplitude history occurs at zero Doppler in the illustration, it need not be the case. The amplitude peak could occur at any angle and is dependent upon the radar and surface geometry. It should also be apparent that the equivalent aperture can be significantly less than the length of time the target is in view because the amplitude history will appear as a weighting function across the aperture. For the Lunar Sounder design, range variations and antenna patterns only have a small effect. Therefore, the

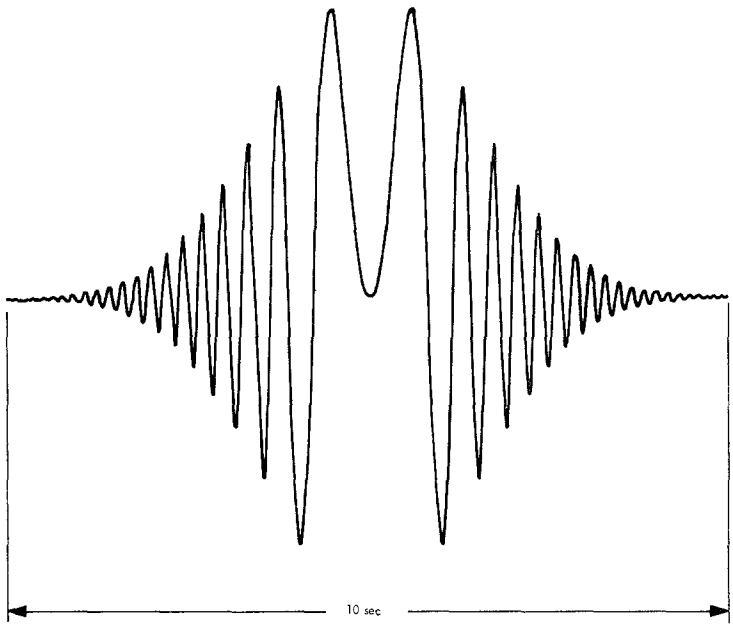

Fig. 1. An example of the Doppler frequency and voltage amplitude histories of a surface target is shown across a 10 s aperture. The signal goes through zero frequency and zero phase and maximum envelope amplitude simultaneously. This situation has been idealized for this illustration and will rarely be the case for real targets. The frequency variation is similar to 5 MHz radar echo. It is apparent that the length of the actual synthetic aperture is a partial function of the target backscatter properties.

effective synthetic aperture is primarily a function of the target backscatter properties.

An example of an actual echo signal is shown in Figure 2. This signal was obtained by the JPL 25 cm coherent radar operating over the ocean from the NASA Ames CV-990 aircraft. The apparent signal-to-noise ratio shown here is very similar to the SNR expected on the Lunar Sounder S-209. The echo is a replica of the transmitted chirped signal because the target area is relatively smooth. This photograph was taken with a Polaroid camera with a setting of 1/30th second and the PRF was about 2 KHz. Hence, about 60 successive echoes are shown superimposed.

The same data were recorded on film in another format by an optical recorder and are shown in Figure 3. The signal amplitude modulates the intensity of a CRT as the spot is swept along a line across the screen. The film is pulled past the CRT sweep and

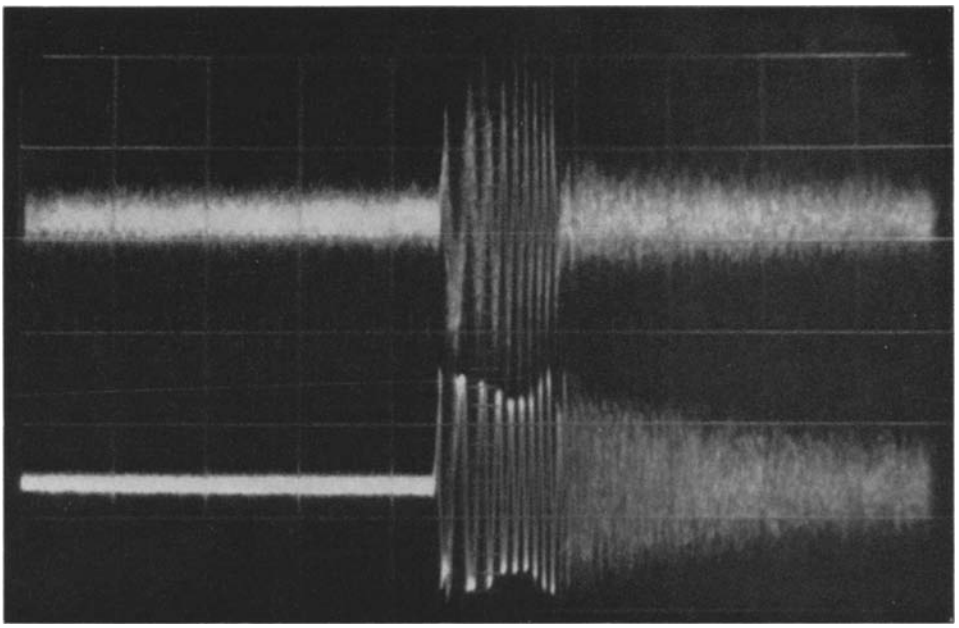

Fig. 2. This photograph of actual radar echoes from a relatively smooth surface shows a cross polarized echo on the upper trace and a direct polarized return on the lower trace. About 60 echoes are superimposed. The data were taken with the JPL 25 cm wavelength radar from the NASA Ames CV990 aircraft at an altitude of about 10 km. The SNR on the upper trace is similar to the SNR expected on the Lunar Sounder. The vertical axis is voltage, the horizontal axis is time. The frequency modulation as seen in the echo is a replica of the transmitted expanded pulse or chirp.

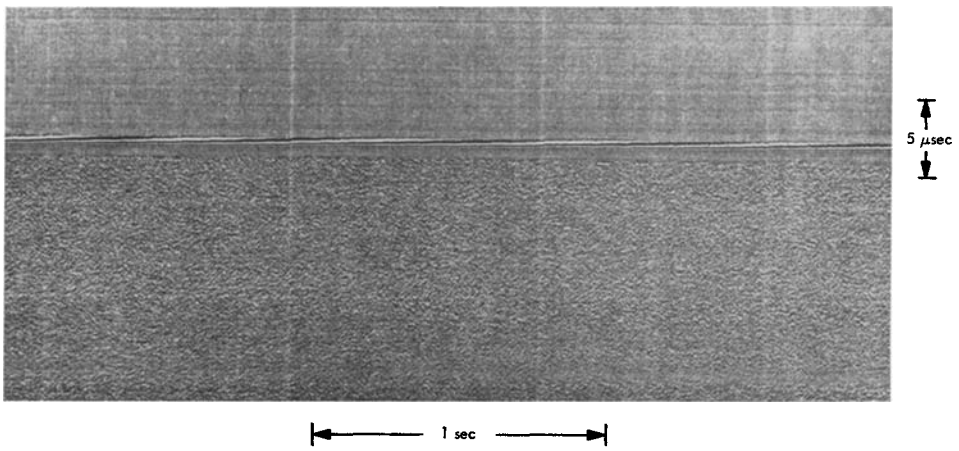

Fig. 3. This section of a range-Doppler pattern of radar echoes was made by recording the intensity modulation of a CRT on a moving film as the aircraft moved. The same chirped signal property as seen in Figure 2 can be seen in the intensity pattern across the short dimension of this figure. During a period of one second the aircraft moved about 250 m and the range changed about one-half wavelength (12.5 cm) as measured by the 360° phase shift. This phase shift can be seen along the long dimension of the figure at the leading edge of the echo.

each echo period produces a line on the film. These lines are overlapping and separate sweeps cannot be seen. The chirp pattern is visible across the short dimension of the figure and the phase change on the leading edge represents a change in range between the radar and the surface. A phase change of 360° is a distance change of $\lambda/2$ or 12.5 cm in this case. This figure illustrates the stability of the radar measurement technique and that a relative range can be measured to within about 2 cm.

The patterns shown in Figure 4 are computer simulations of the Lunar Sounder performance. The case illustrated is for a range rate of change of 10 m per kilometer. It can be seen that the Lunar Sounder will be a sensitive slope detector.

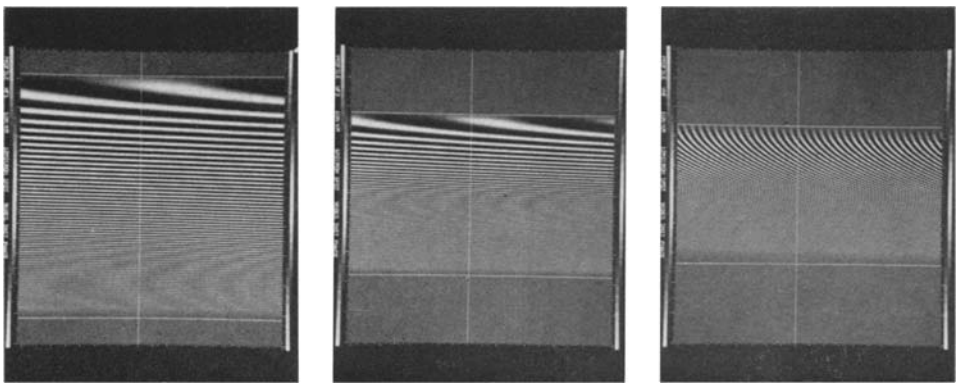

Fig. 4. A computer printout of the expected range-Doppler patterns for the Lunar Sounder radars shows the effect of relative range change of 10 m per kilometer. The equivalent Doppler frequencies are 0.53 Hz, 1.6 Hz and 16 Hz.

As the surface becomes more irregular, variations in the patterns will occur, the lines in the pattern will become jagged. If the amplitude of the signal decreases and the pattern is retained, then the cause of the amplitude decrease would be a decrease in dielectric constant. If the pulse-to-pulse phase jitter increases with a decrease in echo amplitude, the most likely cause is an increase in surface roughness at the sub-radar point.

Both Figures 3 and 4 are examples of radar echo amplitude and phase patterns as they are recorded by an optical recorder. When these patterns are acquired with an antenna pattern that looks to one side of the sub-radar track and the optical recorder film is then processed on an optical correlator, the result is a range-azimuth (angle) radar image of the surface. An example of the image data format is shown in Figure 5. These data are similar to side-looking radar data but they also include the vertical incidence reflection. The profile of the terrain generally appears as a bright line and is located directly beneath the aircraft. Regions or targets located farther to the right of the aircraft track are displayed at a greater distance from the profile line. The basic procedures for this type of processing are well known and have been used for processing side-looking radar data for many years. (Brown, 1966; Leith, 1968) The image shown

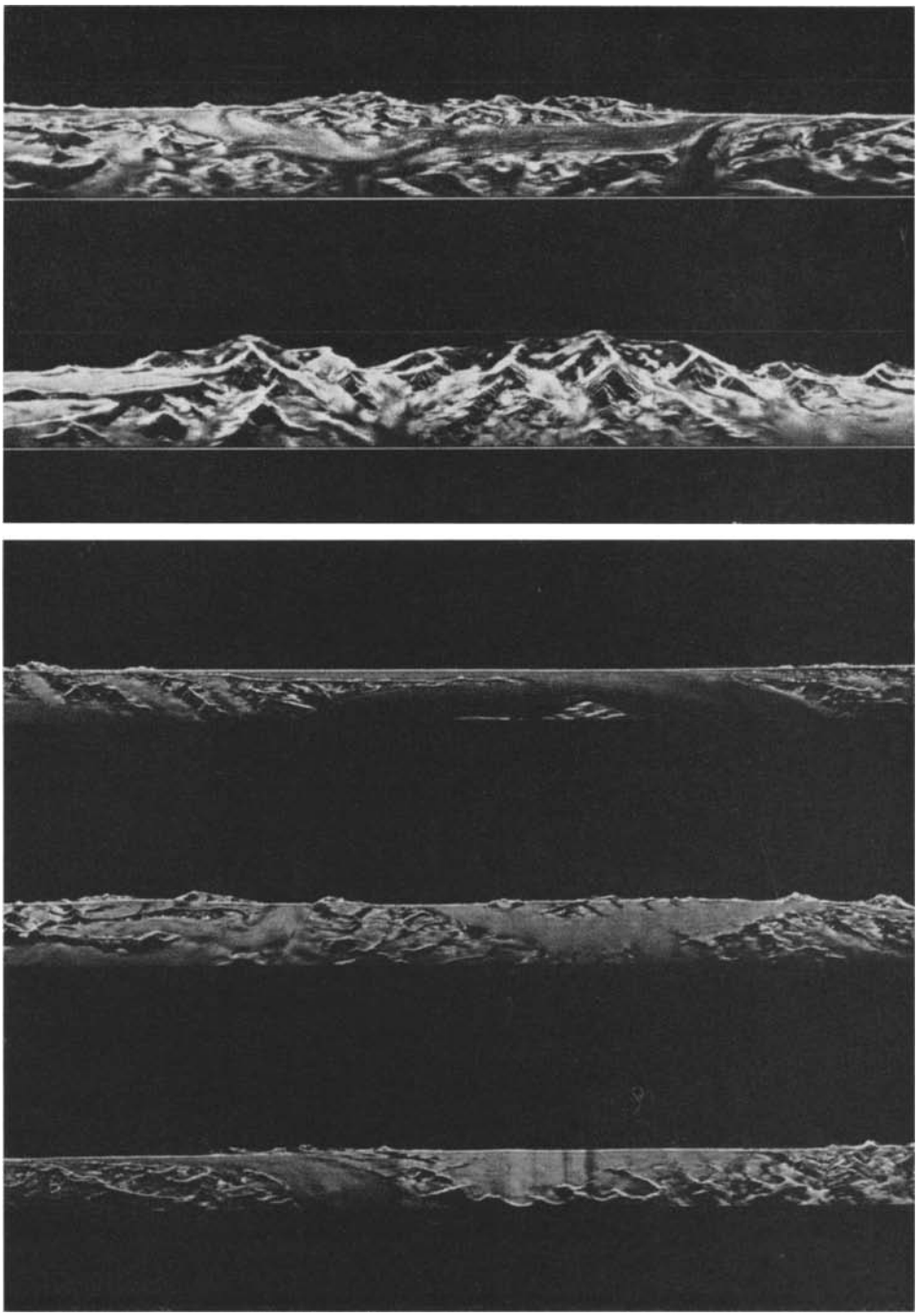

Fig. 5. A typical radar image as derived from the range-Doppler patterns similar to those shown in Figure 3 shows the profile of the terrain directly beneath the aircraft as well as the areas off to one side. The radar image is a range-angle image as compared with usual angle-angle image seen in a photograph. The cross-track dimension is approximately 9 km and covers angles of 0 to 50° off-vertical. Along the track the dimension is 75 km. The resolution of the radar was about 100 m in azimuth and 15 m in range. The morains in the Walsh Glacier were covered by 10 m of snow. The upper Seward Glacier is identified by a vertical banding. These data were acquired by the JPL 25 cm radar and processed by the University of Michigan.

in Figure 5 was obtained with the JPL 25 cm radar and processed by the University of Michigan. The regions imaged are located in the southeastern section of Alaska.

There are indications of subsurface features in the upper Seward Glacier at depths of 100 to 200 m. However, no special attempt has been made to detect the presence of subsurface features in the glacial imagery or to verify their presence.

To summarize the *surface* properties measurements, the Lunar Sounder will use coherent radar techniques to do the following:

(1) Measure the range to the surface with an accuracy of 5 to 50 cm with respect to the spacecraft position.

(2) Resolve two targets separated in distance by 10 radar frequency wavelengths.

(3) Locate single targets along track to within 5 radar frequency wavelengths with respect to the spacecraft position.

(4) Measure variations in surface dielectric constant and separate the surface roughness effects.

(5) Provide surface areal resolutions on the order of 5 by 60 wavelengths at 20° off vertical.

(6) Provide a profile of the lunar surface for a traverse length that is as long as the sub-spacecraft track for two consecutive orbits.

3. Detection of Subsurface Discontinuities in Dielectric Constant

A most intriguing aspect of the radar is the potential capability for detecting subsurface dielectric discontinuities. Features such as a regolith-rock type interface may exist within 1 km of the surface and can be detected by various measurement techniques. Because the *a priori* information about the subsurface electrical properties is so meager, the key point in the experiment design is to record as much about the echo as possible. The reason that the echo amplitude and phase of each echo are recorded with wide bandwidth and wide dynamic range is to minimize the loss of unexpected information about the subsurface. When the data as recorded on film are returned, sophisticated data reduction and filtering techniques will be used to locate the subsurface dielectric discontinuities.

The most straightforward way to detect a subsurface feature is in the time domain where the second surface appears as a second echo and there are no surface features of the same configuration at the same range. Under these conditions the echo amplitude in the lower half of the band can be compared with the echo amplitude in the upper half of the band, and the average loss tangent of the layer is determined in the Appendix as

$$\tan \delta = \frac{S_2 - S_1}{27.2 (f_2 - f_1) \tau}, \tag{3.1}$$

where S_1 and S_2 are the measured subsurface echo amplitudes for the lower and upper half of the bands respectively. The premise is made that the variation in $\tan \delta$ is a second order effect for a 5% variation in frequency. This measurement technique can be used in areas where the surface and the subsurface layers are relatively smooth.

A second method for detecting a subsurface feature is for the case where the subsurface and surface are within a single pulse width (or resolution element). In this case, the two echoes mix together and cause a modulation of the chirp envelope. This technique is equivalent to the frequency domain measurement that is often used in surface EM sounding. Examples of the echo waveforms are given in Figures 6 and 7.

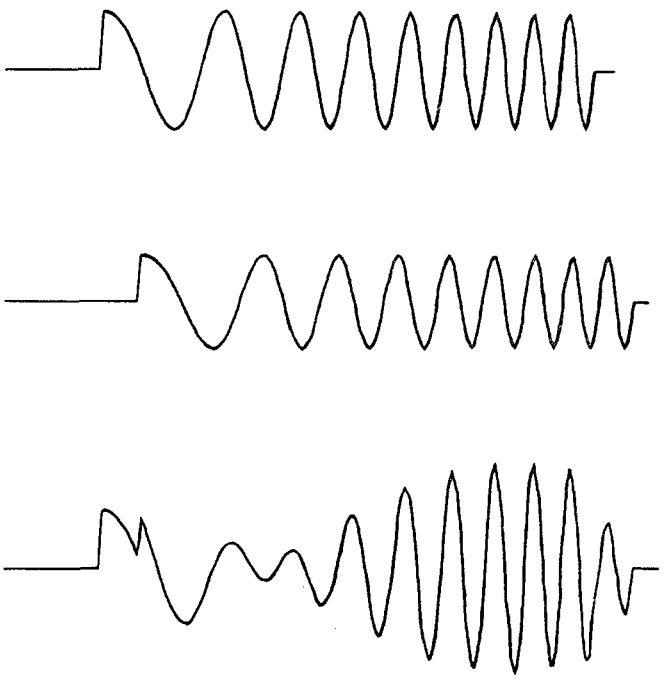

Fig. 6. These plots are voltage versus time and show the addition of two chirp signals that are displaced slightly in time. The amplitude variation provides a sensitive technique for detecting a subsurface layer that is within the pulse resolution time.

Figure 6 shows an exaggerated case of two echoes adding whereas Figure 7 shows a simulated lunar sounder case for the 5 MHz channel (nominal resolution of 300 m in material where $\varepsilon = 4$) and the subsurface layer at 100 m below the first surface. Again, this technique is only useful in areas where the surface is relatively smooth.

A third method for detecting subsurface features, and one that can provide unambiguous results in areas where the surface is irregular, employs the geometry of two consecutive orbits. The situation is illustrated in Figure 8. The subsurface feature, B, is observed on each orbit. When the data are processed the feature is located on a reference surface at B' and B''. The imagery for each orbit is converted to orthographic coordinates and compared using a known surface feature, A, as a reference. Features that are displaced toward the sub-radar track are above the reference surface and those displaced away from the track are below the surface. A computer sequence can be used to print only those features of interest. The amount of displacement is proportional to the product $D\sqrt{\varepsilon}$ (depth · index of refraction).

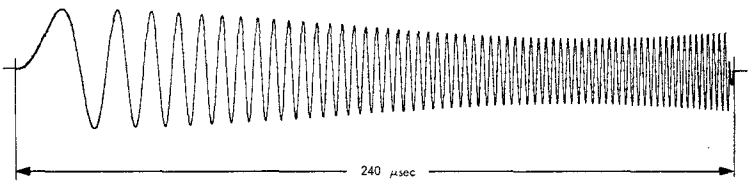

Fig. 7. This pattern of the chirp for the Lunar Sounder 5 MHz radar shows the result of a subsurface located 100 m below the surface. The resolution of this radar is about 300 m in the surface layer material.

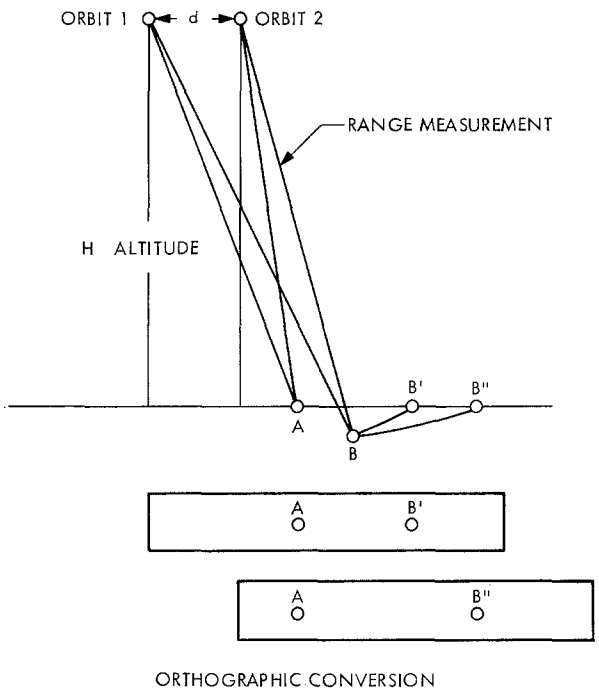

Fig. 8. A technique for detecting subsurface features uses the geometry involved with the observation of the subsurface target on successive orbits. The spacecraft velocity vectors are normal to the page. A comparison of the two corrected (orthographic) images will show the features displaced when they are not in the reference plane. For example, target B appears as B' and B'' on the images where A, a known surface feature, has been used to establish a reference plane. When the two images are compared by superimposing the A target, the B target will be displaced. The direction and distance of displacement indicate whether B is above or below the reference plane and the distance (in time delay). If the dielectric constant of the propagating medium is known, then the depth of B can be determined.

The expected performance of the coherent radar in detecting subsurface features is related to six factors: (1) the electrical losses in the intermediate surface material and the dielectric discontinuities; (2) the introduction of phase errors in the echo caused by variations in the refractive index over the coherent aperture; (3) scattering losses in the intermediate surface material; (4) the backscattering function of the surface,

subsurface, and intermediate material; (5) the sidelobe levels of the transmitted radar pulse as processed by the radar system; (6) the dynamic range of the radar system.

The electrical loss is determined in the Appendix to be (in dB)

$$L = 27.2 f\tau \tan\delta \tag{3.2}$$

where $\tan\delta$ is the loss tangent; f is the frequency of propagation; τ is the delay beyond the first surface echo.

The values of $\tan\delta$ published by Collett and Katsube (1971) were used for all performance calculations. The ratio of surface to subsurface echo strength is

$$\frac{R_{01}}{R_{\text{eff}}} = \frac{1}{R_{12}(1-R_{01})^2}\, 10^{27.2 f\tau \tan\delta}, \tag{3.3}$$

where R_{01} = 1st surface reflectivity (power); R_{12} = 2nd surface reflectivity (power).

The threshold of detection was designed to be 65 dB for the S-209 experiment.

The introduction of phase errors reduces the ability of the coherent radar system to add the successive echo amplitudes in a totally linear fashion and this reduction in coherence acts as a loss. There are three major contributors to the phase error, the surface irregularities, dielectric constant variations and random errors. Each contribution provides a probability distribution of phase shifts that deviate from the ideal case of planar surfaces and a homogeneous dielectric material. The phase shift caused by the surface is a function of the surface displacement from the mean surface

$$\Delta\theta = (2\pi/\lambda)\, s, \tag{3.4}$$

where s is the deviation in elevation of the surface from a planar or spherical reference.

The phase shift (two way) for the dielectric constant variations is given by

$$\Delta\theta = \frac{2\pi}{\lambda} \cdot D\sqrt{\varepsilon} \cdot \frac{\Delta\varepsilon}{\varepsilon}, \tag{3.5}$$

where D = depth of subsurface feature; ε = relative dielectric constant; $\Delta\varepsilon$ = variation in ε as averaged along a propagation path; λ = free space wavelength.

The effect of random phase errors on performance is currently being evaluated. As a worst case, the successive echoes will add as the square root of the number rather than linearly and the SNRI as listed in Table II will be reduced by a factor of two, and the maximum depth of penetration will be reduced by about 30%.

Additional losses can result from scattering of energy when the intervening layer has a large faction of dielectric constant variations that are about the size of 0.1 λ (λ in material). The significance of these losses depends on the magnitude of dielectric discontinuity and the number of scatterers and this loss mechanism is also being studied.

Although there are factors that tend to mask the detection of subsurface features, it is expected that the surface conditions of the Moon will be sufficiently varied and in some areas their effect will be small. In addition, the data reduction techniques can employ optimum filtering techniques to enhance subsurface feature patterns. The use

of optimum filtering is possible because the coherent radar is basically a linear system that preserves the amplitude and phase of each echo.

The 150 MHz radar on the S-209 experiment is expected to determine the depth of the regolith. The nominal penetration is 10 to 150 m for a dielectric constant ratio of 1 to 1.3 at the base of the regolith. A depth less than 10 m may be measured by the modulation envelope method. The 15 MHz radar is designed to detect features in the range of 80 m to 800 m and the 5 MHz radar, 300 to 1000 m. These estimates are based upon the loss tangent measurements made by Collett and Katsube (1971) on the lunar samples returned. Insofar as the electrical losses are concerned, the depth of penetration is directly proportional to the loss tangent. If the loss tangent is lower by a factor of two, the 5 MHz system will penetrate to 2000 m or conversely, if tan δ is a factor of two higher, then the depth of observation will be 500 m.

There may be subsurface structures that are detectable which are located near the boundaries of the mare and terrae. In these regions a wide range of depths of dielectric discontinuities may be expected. Such areas could serve as a form of calibration for all three radar sounding systems. In addition, the geological interest in subsurface structure is relatively high for these regions.

For the most part, the discussion in this paper and the radar system design have been based upon the detection of rather subtle changes (for example $\varepsilon_1 = 5$, $\varepsilon_2 = 8$) in dielectric constant. Larger changes such as those caused by voids, major mineral deposits or water would, of course, be easier to detect. Although the probability of occurrence of these subsurface phenomena may be low, the region of the Moon surveyed will be four circumlunar great circle tracks, hence, the potential for discovering something new about the lunar subsurface is considered to be significant.

Acknowledgements

The author wishes to thank R. Jordan, T. Thompson and R. Phillips for their help in preparing and reviewing this paper. This paper presents the results of one phase of research carried out at the Jet Propulsion Laboratory, California Institute of Technology, under Contract NAS 7-100, sponsored by the National Aeronautics and Space Administration.

An Investigator Team is responsible for the scientific investigation related to the Apollo Lunar Sounder Experiment, S-209. The team membership includes the following:

Jet Propulsion Laboratory: W. Brown, Principal Investigator; R. Phillips, Co-Investigator, Team Leader; T. Thompson; and R. Jordan.

University of Utah: S. Ward, Principal Investigator; W. Peeples; and J. Ryu.

Unites States Geological Survey: R. Eggleton, Co-investigator; and G. Schaber.

University of Michigan: L. Porcello, Co-investigator; G. Adams; P. Jackson; and J. Zelenka.

NASA/Manned Spacecraft Center: V. Dauphin.

NASA/Ames Research Center: W. Linlor, Co-investigator.

References

Brown, W. M.: 1967, *IEEE Trans. Aerospace Electr. Syst.* Vol. AES-3, No. 2, March 1967.
Collett, L. S. and Katsube, T. J.: 1971, *Geochim. Cosmochim. Acta,* Suppl. 2, Proceedings of the Second Lunar Science Conference, Vol. **3**, 2367–2379.
Leith, E. N.: 1968, *IEEE Trans. Aerospace Electr. Syst.* Vol. AES-4, No. 6, November 1968.

Appendix

A. THE RANGE ERROR EQUATION (2.1)

The slope of the transition response to step function of amplitude A for a bandpass filter of bandwidth, B is approximated by

$$\text{Slope} \simeq A \cdot B .$$

The Gaussian noise added to the step function with a deviation of σ_N, will cause a jitter or uncertainty in the time that step function will pass through the threshold at $A/2$. The deviation of the uncertainty is σ_τ. Then

$$\text{Slope} = A \cdot B = \frac{\sigma_N}{\sigma_\tau},$$

where σ_N is small with respect to A.

The range error is given by

$$\sigma_R = \frac{c}{2} \cdot \sigma_\tau = \frac{c}{2} \cdot \frac{\sigma_N}{A \cdot B} .$$

where c is the velocity of propagation.

However,

$$\frac{A}{\sigma_N} = (\text{SNR})^{1/2} ;$$

therefore

$$\sigma_R = \frac{1}{B(\text{SNR})^{1/2}} (c/2) .$$

B. THE LOSS TANGENT EQUATION (3.1)

The loss in signal power in dB versus delay is

$$L = 27.2 \cdot f\tau \tan\delta .$$

When the same feature is observed on two frequencies, the amplitudes will differ.

The amplitude S, in dBw, plus the loss in dB is a constant. Hence,

$$S_1 + L_1 = S_2 + L_2 ,$$

or

$$S_1 + 27.2 \tan\delta f_1 = S_2 + 27.2 \tan\delta f_2 ,$$

or

$$\tan\delta = \frac{S_2 - S_1}{21.2\,(f_2 - f_1)\,\tau}.$$

The time delay and loss tangent are assumed to be the same for both frequencies. The intent is to process the upper and lower segments of the band separately.

C. THE SUBSURFACE ELECTRICAL LOSS EQUATION (3.2)

The attenuation of an electromagnetic signal in a material with a dielectric constant of ε and a loss tangent of $\tan\delta$ is given by the equation

$$\frac{\text{Power out}}{\text{Power in}} = \exp\left[-\frac{2\pi\tan\delta\cdot\sqrt{\varepsilon}\cdot 2z}{\lambda_0}\right],$$

where $2z$ is the two way path length through the lossy material, λ_0 is the free space wavelength.

In dB, the loss is given by

$$\text{Loss} = 10\log\frac{\text{Power in}}{\text{Power out}} = 4.32\cdot 2\pi\cdot\tan\delta\cdot\frac{\sqrt{\varepsilon}\cdot 2z}{\lambda_0}.$$

The time delay is

$$\tau = 2z\sqrt{\varepsilon}/c = 2z\sqrt{\varepsilon}/\lambda_0 f\,.$$

Hence

$$\text{Loss} = 27.2\cdot f\tau\tan\delta\,.$$